Photochemical & Photobiological Sciences

PAPER

Fluorescent imidazole-based chemosensors for the reversible detection of cyanide and mercury ions†

Ganapathi Emandi,[a] Keith J. Flanagan[a] and Mathias O. Senge ⃰[a,b]

We report 4-(2-(5-(*tert*-butyl)-3-formyl-2-hydroxyphenyl)-1*H*-phenanthro[9,10-*d*]imidazol-1-yl)benzoic acid **1** and 4-(2-(5-(*tert*-butyl)-3-formyl-2-hydroxyphenyl)-4,5-diphenyl-1*H*-imidazol-1-yl)benzoic acid **2** as reversible luminescent sensors for the detection of cyanide and mercury ions. These imidazole derivatives were characterized using spectroscopic techniques and single crystal X-ray crystallography. The compounds showed sensing exclusively towards CN^- ions, which resulted in the quenching of fluorescence and a decreased singlet state life time. The detection limit of imidazole derivatives **1** and **2** were found to be 0.8 μM and 1.2 μM respectively, in a CH_3CN/H_2O system. Job's plot analysis, ^{1}H NMR spectra and LC-MS studies supported the formation of the respective cyanohydrin. This cyanohydrin was further used as a reversible sensor for the detection of Hg^{2+} ions through metal-assisted elimination. The reversibility and reusability of sensors for the detection of CN^- and Hg^{2+} ions were tested for four consecutive cycles.

Introduction

The coordination chemistry of anions and metals has gained significant attention in recent times due to its relevance to ecology, health and other areas.[1] Especially the development of fluorescent sensors and molecular receptors for the detection of chemical species for biological, environmental and security applications is a contemporary area of interest.[1] Among the anions, cyanide is extremely toxic and deleterious to human health, causing vomiting, convulsions, loss of consciousness, and eventually leads to death.[2] According to the World Health Organization, the maximum acceptable level of cyanide in drinking water is 1.9 μM.[3] Due to the increased use of cyanide in many products and processes ranging from plastic, fibers, gold, dyes, chelating agents for water treatment, to pharmaceuticals it poses a significant threat to life.[2a,4] Likewise, among the dangers of various heavy metal ions, mercury ranks the highest due to its deleterious effects on human health and environmental impact.[5] Even at very low

concentrations the Hg^{2+} ion is extremely toxic to living creatures and can affect various organs of the body, including the nervous system due to the ease of membrane passage of Hg^{2+} and some of its derivatives.[6]

Therefore, it is desirable to develop sensitive, selective and practical methods to monitor the very low concentration of cyanide/mercury from contaminant sources and drinking water and in possible security scenarios.[1k,l] Although many chemical and physiochemical methods (chromatography, electrochemical analysis, *etc.*) have been developed for the detection of cyanide their practical applications have been limited due to difficulties in sample preparation, complicated measurements, and low sensitivity.[7] Optical chemosensors for cyanide have attracted considerable attention in the last decades due to their simplicity and rapid measurements.[8] Among various detection techniques, fluorescence detection is the most attractive as it offers several advantages including high sensitivity, the simplicity of operation and non-invasiveness.[9] Accordingly, significant efforts have been expended on the development of fluorescent sensors for cyanide.[10] As cyanide is a good nucleophile this characteristic can be used as a basis for the development of chemodosimetric probes in aqueous or semi-aqueous solutions.[10e]

Fluorescent dyes based on excited-state intra-molecular proton transfer (ESIPT) have emerged as a promising class of materials for many practical applications such as optical sensors,[11] switches,[12] laser dyes,[13] and white light OLEDs.[14] For example, Lochbrunner *et al.* explored the concept of ESIPT by using 2-(2-hydroxyphenyl)-benzothiazole (HBS) and 2-(2-

[a]*SFI Tetrapyrrole Laboratory, School of Chemistry, Trinity Biomedical Sciences Institute, 152-160 Pearse Street, Trinity College Dublin, The University of Dublin, Dublin 2, Ireland*
[b]*Medicinal Chemistry, Trinity Translational Medicine Institute, Trinity Centre for Health Sciences, Trinity College Dublin, The University of Dublin, St James's Hospital, Dublin 8, Ireland. E-mail: sengem@tcd.ie*
†Electronic supplementary information (ESI) available: Details of spectroscopic and crystallographic studies. CCDC 1821473 and 1821472. For ESI and crystallographic data in CIF or other electronic format see DOI: 10.1039/c8pp00226f

hydroxyphenyl)-benzoxazole (HBO) moieties.[15] Subsequently, many HBO and HBS derivatives were studied for their application in biological systems, as anion sensors, and in the fabrication of light-emitting devices.[11–14] 2-(2-Hydroxyphenyl)-benzimidazole (HBI) derivatives have much higher quantum yields and show better sensitivity towards anions or cations in protic/polar solvents compared to HBO/HBS derivatives.[16]

Based on this advantage, benzimidazole derivatives have become attractive targets in optical sensing and material studies.[17] In this context, we were interested to explore the potential of imidazole-based reversible chemosensors for the detection of cyanide and mercury ions. Herein, we describe the development of 4-(2-(5-(tert-butyl)-3-formyl-2-hydroxyphenyl)-1H-phenanthro[9,10-d]imidazol-1-yl)benzoic acid 1 and 4-(2-(5-(tert-butyl)-3-formyl-2-hydroxyphenyl)-4,5-diphenyl-1H-imidazol-1-yl)benzoic acid 2 reversible chemosensors. The results show these derivatives can act as reversible sensors for the detection of cyanide and mercury ions in acetonitrile/water media.

Results and discussion

Synthesis and characterization

The desired target compounds 1 and 2 were synthesized in a two-step reaction as shown in Scheme 1. In the first step, compounds 3 and 4 were obtained by refluxing phenanthrene-9,10-dione/benzil, 5-tert-butyl-2-hydroxyisophthalaldehyde, ethyl 4-aminobenzoate and ammonium hydroxide in glacial acetic acid by following standard reported procedures in the literature.[18] Compounds 3 and 4 were isolated by using column chromatography techniques and characterized by ^{1}H NMR spectroscopy and mass spectrometry. In the second step, one equivalent of the respective esters 3 and 4 were treated with an excess amount of potassium hydroxide in THF : MeOH (1 : 1) and refluxed for 6 h. TLC analysis indicated the disappearance

of the less polar imidazole esters 3 and 4 and the appearance of more polar fluorescent spots corresponding to the desired 4-(2-(5-(tert-butyl)-3-formyl-2-hydroxyphenyl) substituted imidazole 1 and 2, respectively. After purification and drying the target compounds were obtained in 90–92% yield. The sensor candidate molecules 1 and 2 were characterized using FT-IR, ^{1}H, ^{1}H–^{1}H COSY and ^{13}C NMR spectroscopy as well as high-resolution mass spectrometry analysis, which are provided in the ESI (Fig. S1–S12†). In the ^{1}H NMR spectra both compounds show signals at around 13.50 ppm and 10.40 ppm corresponding to the hydroxy and aldehyde protons, respectively. Other signals at δ = 8.92 to 7.00 ppm can be assigned to the aromatic protons of the imidazole moiety and the tert-butyl group is identified by a singlet at 0.98 ppm. A comparison of normalized absorption and emission spectra of compounds 1 and 2 is presented in Fig. 1 and the corresponding data are presented in Table S1 (ESI†). The main absorption bands of compounds 1 and 2 were observed at 370 nm and 345 nm respectively. Both compounds 1 and 2 showed a strong fluorescence at 495 nm and 491 nm with a quantum yield of
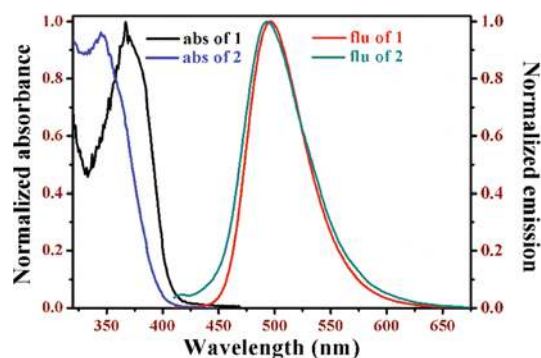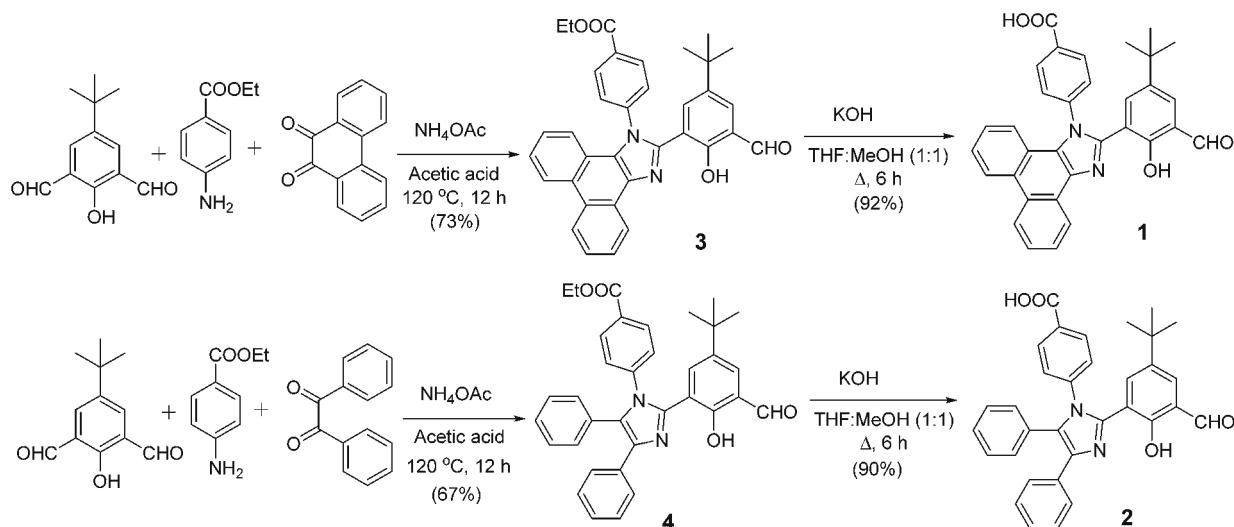

Fig. 1 Comparison of normalized absorption and emission spectra of compounds 1 and 2 recorded in CH$_3$CN/H$_2$O (1 : 1) (10 μM).

Scheme 1 Synthesis of 4-(2-(5-(tert-butyl)-3-formyl-2-hydroxyphenyl) substituted imidazoles 1 and 2.

Φ = 0.19 for compound **1** and Φ = 0.12 for compound **2**. Upon photoexcitation the singlet excited state of the enol form is populated and then an ultrafast excited-state intra-molecular proton transfer (ESIPT) process occurs and the keto form at the singlet state can be generated, which can be stabilized with an intramolecular hydrogen bond. As the ESIPT process is much faster than the fluorescence process the observed fluorescence for the ESIPT chromophore is presumably due to the keto tautomer.[12b] The singlet state lifetimes of compounds **1** and **2** were 4.6 ns and 3.9 ns, respectively.

Single crystal X-ray structure determinations

Single crystals suitable for determination by X-ray diffraction of compound **4** and **2** were obtained by slow evaporation of
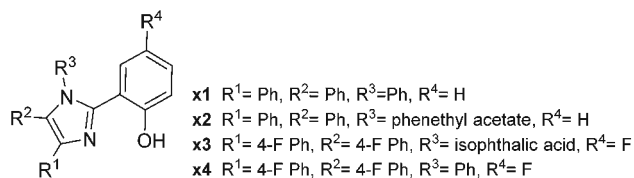

Fig. 2 Literary crystal structures used in comparison to compounds **2** and **4**.

CH_2Cl_2/hexane and dimethyl sulfoxide, respectively using standard techniques.[19] Compound **4** crystallized in the triclinic space group $P\bar{1}$. As shown in Fig. 3a, four different kinds of weak interactions were observed. A short intramolecular interaction, N2···H3–O3 (1.6412(8) Å), was observed between the alcohol group and the imidazole ring. A weak hydrogen-bonded network was seen between O3···H11–C11 (2.5064(1) Å), O3···H10–C10 (2.5355(2) Å) and O4···H20–C20 (2.5902(1) Å) and is involved in an offset stacking pattern of the molecules (see Fig. 3b).

Compound **2** crystallized in the monoclinic space group $P2_1/c$ as a DMSO solvate. Due to the free acid group, a hydrogen-bonded network is formed between the benzoic acid–DMSO–aldehyde groups (O2–H2···O1s (1.7429(1) Å) and C2s–H2sc···O4 (2.3406(1) Å) to form head-to-head dimers, as shown in Fig. 3c. An additional short intramolecular interaction is present between N2···H3–O3 (1.7184(1) Å). As seen in Fig. 3d, there is a head-to-tail overlap between the imidazole moieties within the packing diagram as a result of weak interactions between the alcohol group and aromatic hydrogen C16–H16···O3 (2.529(6) Å).

When considering the imidazole plane of compound **2** and **4** there is a noticeable variation between the rotation of substituted phenyl rings at R[1] (ring 1), R[2] (ring 2), R[3] (ring 3), and
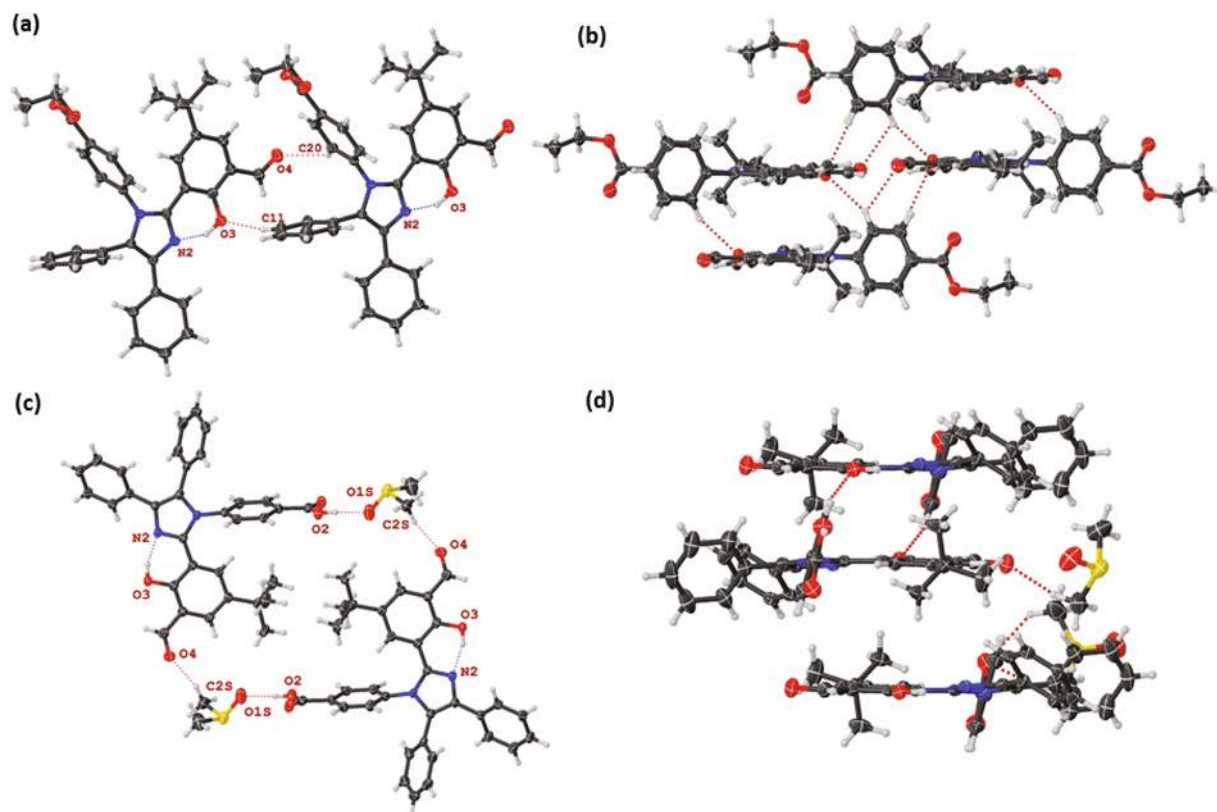

Fig. 3 Crystal structure of (a) compound **4** (ellipsoids indicate thermal displacement 50%) showing intramolecular interactions N···H (blue dashed line) and intermolecular interactions OH···H–phenyl and CHO··· H–phenyl (red dashed line) and (c) compound **2** (ellipsoids indicate thermal displacement 50%) showing hydrogen-bonded network between benzoic acid–DMSO–aldehyde (red dashed line) and intramolecular interactions N···H (blue dashed line). (b) and (d) compound **4** and compound **2** (thermal displacements 50%) showing stacking between imidazole layers.

1452 | *Photochem. Photobiol. Sci.*, 2018, **17**, 1450–1461

This journal is © The Royal Society of Chemistry and Owner Societies 2018

Table 1 Rotation of substituted phenyl rings shown in Fig. 2 with regards to the imidazole plane

	4	2	x1_1	x1_2	x2	x3_DMF, EtOH	x3_MeOH	x3_DMF	x3_DMF, IPA	x3_1	x3_2	x4
Ring 1	11.3(6)	39.7(1)	3.4	28.2	25.4	12.1	9.2	12.3	11.2	11.8	36.5	28.7
Ring 2	88.9(5)	51.3(2)	83.9	88.8	61.7	71.4	84.1	71.0	66.0	77.0	68.3	57.9
Ring 3	86.7(3)	71.3(9)	89.8	82.3	84.0	76.3	61.4	76.0	63.5	83.6	66.8	78.0
Ring 4	1.7(6)	9.2(3)	3.0	6.8	2.2	22.1	24.7	22.7	28.4	7.0	14.6	6.1

2-hydroxyphenyl moiety (ring 4), as seen in Fig. 2 and Table 1. Compound **4** shows the greatest degree of planarity with both ring 1 and ring 4 being rotated at 11.3(6) and 1.7(6)° with regards to the central imidazole moiety. Conversely, ring 2 and ring 3 show an almost orthogonal to the imidazole plane at 88.9(5) and 86.7(3)° respectively. Compound **2** shows a larger rotation of ring 1 and ring 4, 39.7(1) and 9.2(3)° respectively. Interestingly, ring 2 and ring 3 show a smaller rotation at 51.3(2) and 71.3(9)°.

In comparison to published X-ray structures outlined in Fig. 2 and Table 1, similar trends can be observed.[18,20] For the structures that do not include a solvent, ring 4 shows the smallest rotational angle to the imidazole plane 1.7–14.6° with ring 1 showing the second smallest rotational angle at 3.4–36.5°. However, the inclusion of solvent appears to reverse this trend with ring 1 showing the smallest angle at 9.2–12.3° and ring 4 exhibiting larger rotation at 22.1–28.4°. Interestingly, the introduction of DMSO to compound **2** does not follow this trend with the ring 4 rotation much smaller than the ring 1 rotation around the imidazole plane. The rotations around ring 2 and ring 3 show a large degree of freedom with rotational angles around the imidazole plane at 57.9–88.8° and 61.4–89.8°, respectively, similar to both compounds **2** and **4**.

Anion sensing studies

Since both compounds **1** and **2** carry aldehyde functionalities we anticipated that cyanide is capable of a nucleophilic attack on the carbonyl groups. Therefore, the anion recognition capability of compounds **1** and **2** was systematically tested by treatment with different anions in CH_3CN–H_2O (1 : 1 v/v) solution (Fig. 4). Thus, we first carried out qualitative tests of compound **1** in CH_3CN/H_2O with various anions such as OH^-, F^-, Cl^-, Br^-, I^-, CN^-, AcO^-, N_3^-, ClO_4^-, $H_2PO_4^-$, HSO_4^- (used as their tetrabutylammonium salts). Interestingly, compounds **1** and **2** were strongly fluoresced in solution under a UV lamp,

but changed to a weakly fluorescent solution only in the presence of cyanide ions. A distinct colour change of solutions was not observed in the presence of any of the other anions tested (Fig. S15 in ESI†).

Next, an absorption spectral titration of compound **1** was carried out by the addition of increasing amounts of cyanide ions in CH_3CN/H_2O (1 : 1; v/v) solution and the observed spectral changes are shown in Fig. 5a. Upon gradual addition of CN^- to compound **1**, the intensity of the initial absorption the band at 370 nm gradually decreased and slowly shifted to a longer wavelength with a concomitant increase in the absorbance at 425 nm with a clear isosbestic point at 392 nm indi-

Fig. 5 Changes in (a) absorption and (b) fluorescence spectra of compound **1** (10 μM) upon titration with CN^- (0–3.0 equiv.) in CH_3CN/H_2O (1 : 1) (λ_{ex} = 370 nm). Insets show: (a) Plot of absorbance vs. $[CN^-]/[1]$ molar ratio for absorbance at 375 and 425 nm, respectively; (b) plot of relative intensity maxima at 495 nm as a function of $[CN^-]/[1]$ molar ratio.
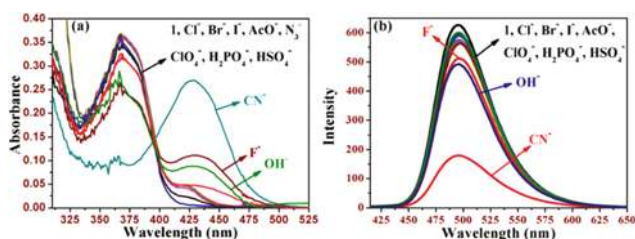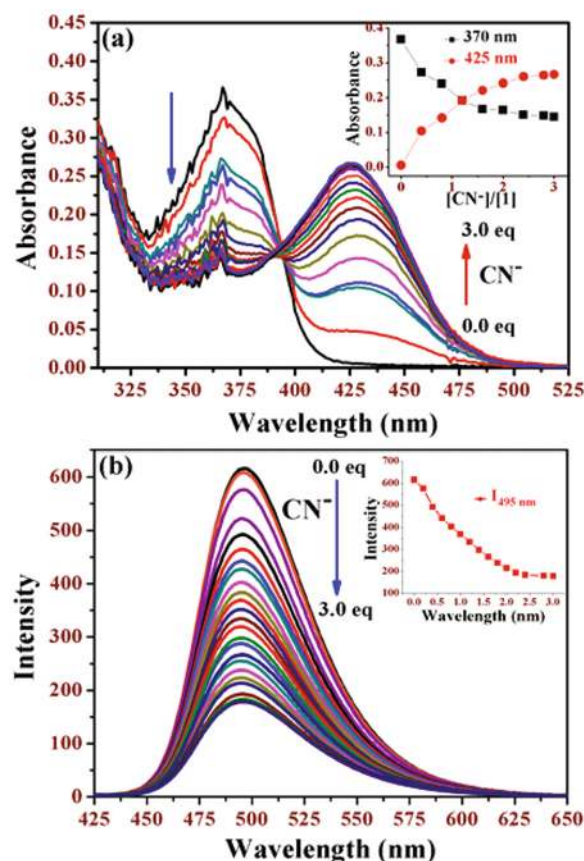

Fig. 4 Changes in (a) absorption and (b) emission of compound **1** (10 μM) upon addition of various anions (10 equiv.) in CH_3CN/H_2O (1 : 1) (λ_{ex} = 370 nm).

cating the presence of two species. The ratio of absorbance at 370 nm (for aldehyde) and at 425 nm (for cyanohydrin derivative) at different equivalents of CN^- ions was plotted and is shown as an inset in Fig. 5a. The significant red-shift in absorption maxima upon addition of CN^- ions to **1** indicates the cyanide ion reacting with the aldehyde group and conversion to the cyanohydrin form. This was accompanied by a clear color change of the solution from colorless to yellow (Fig. S15 in ESI†).

Similarly, the addition of increasing amount of CN^- to a solution of compound **2** resulted in the decrease of the absorption band at 345 nm and the appearance of the new band at 403 nm with one clear isosbestic point at 367 nm. These observations support the cyanohydrin (**2**-CN^-) formation in solution (Fig. S16 in ESI†).

We also investigated the binding phenomenon of CN^- ions to compounds **1** and **2** systematically by fluorescence titration experiments. As shown in Fig. 5b, upon addition of increasing equivalents of CN^- ions, the fluorescence band at 495 nm of sensor **1** gradually decreased up to 3.0 equivalents of CN^- ions and the fluorescence color of the solution changed from strong green fluorescent to weak fluorescent light green as shown in Fig. S15 in ESI.† Incremental addition of CN^- to compound **1** resulted in gradual fluorescence quenching at 495 nm and was saturated at 3.0 equivalents. A fluorescence quenching factor of up to 4-fold for compound **1** upon addition of three equivalents of CN^- was achieved. Similar observations were observed in case of compound **2**. The fluorescent band at 490 nm gradually decreased with increasing the amount of CN^- ions in CH_3CN/H_2O (1 : 1; v/v) solution (Fig. S17 in ESI†). This fluorescence quenching was mainly due to the phenolic OH not participating in a hydrogen bond interaction with the imine nitrogen; it forms a hydrogen bond with the carbonyl oxygen upon cyanohydrin formation; hence, the ESIPT process was ruled out.

To determine the binding stoichiometry, we carried out emission titration experiments in the presence of varying mole-fractions of CN^- in CH_3CN/H_2O medium (Fig. S18 and S19 in ESI†). Job's plot analyses of changes in the emission revealed a maximum at 0.5, indicative of the formation of a 1 : 1 cyanohydrine derivative between imidazole **1** and **2** with CN^- ions. This agrees with the LR-MS mass spectrum obtained for the {**1**-CN^-} adduct (Fig. S20 in ESI†). The association constant of imidazole **1** and **2** by CN^- ions were estimated by the standard Benesi–Hildebrand equation, and the corresponding association constant, K was found to be 8.74 (± 0.77) $\times 10^4$ M^{-1} for compound **1** and 4.36 (± 0.31) $\times 10^4$ M^{-1} for compound **2** (Fig. S21 in ESI†).

The sensitivity of compounds **1** and **2** for the CN^- ions was further evaluated in fluorescence titration profiles, which demonstrated that compounds **1** and **2** have a detection limit of 0.8×10^{-6} M and 1.2×10^{-6} M for the CN- anion, which is lower than the WHO guideline of 1.9 μM cyanide (Fig. S22 and S23 in ESI†).[3] Upon addition of increasing equivalents of CN^- ions (0 to 3.0 equiv.), the singlet excited state lifetime was decreased from 4.6 ns to 1.9 ns (Fig. 6a) and from 3.9 ns to
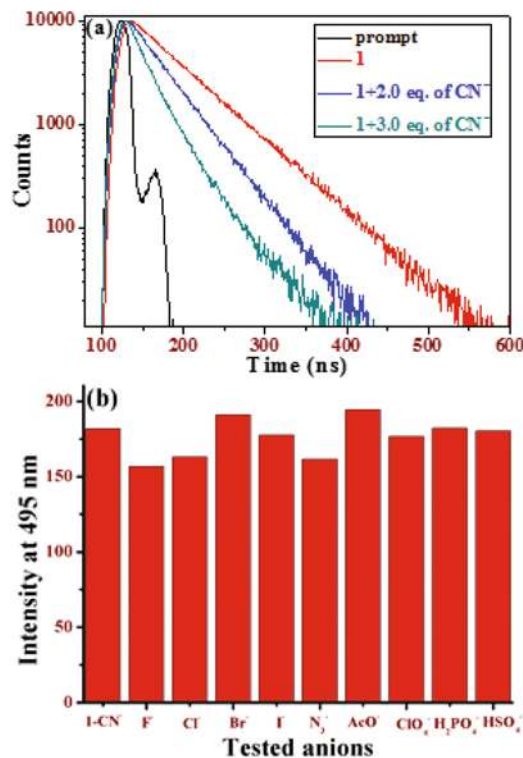

Fig. 6 (a) Time-resolved fluorescence decay profiles of **1** (10 μM) in CH_3CN/H_2O (1 : 1 v/v) solution upon titration with different concentrations of CN^- ions. The excitation wavelength used was 370 nm and emission were detected at the emission-peak maxima (495 nm). (b) Fluorescence intensity of **1** (10 μM) upon the addition of 5.0 equiv. CN^- in the presence of 10.0 equiv. background anions in CH_3CN/H_2O (1 : 1 v/v) λ_{ex} = 370 nm.

1.6 ns for compounds **1** and **2** respectively. To demonstrate the selectivity of compound **1** toward CN^-, competitive anion binding studies were carried out. As shown in Fig. 6b, the fluorescence intensity of {**1**-CN^-} remained unchanged even in the presence of an excess of other anions. The fluorescence titration studies carried out in the presence of other anions, viz., F^-, Cl^-, Br^-, I^-, N_3^-, AcO^-, ClO_4^-, $H_2PO_4^-$ and HSO_4^- showed no change in the original emission intensity of {**1**-CN^-}, suggesting the imidazole {**1**-CN^-} does not sense these anions (Fig. 6b).

In order to evaluate the formation of the cyanohydrin from an aldehyde, ^1H NMR titration studies were carried out between compound **1** and CN^- in DMSO-d_6 solvent and the spectra are shown in Fig. 7. The ^1H NMR spectrum of compound **1** showed two characteristic peaks, one at 13.50 ppm (OH) and another at 10.40 ppm (CHO). During the titration, the concentration of compound **1** was kept constant and upon gradual increase of CN^- concentration, the most noticeable change was observed for the signal of the aldehyde proton at 10.50 ppm, which was shifted upfield to 5.95 ppm which corresponds to the formation of the cyanohydrin. The hydroxy proton at 13.50 ppm was shifted slightly downfield to 14.10 ppm which is due to the hydrogen bonding interaction
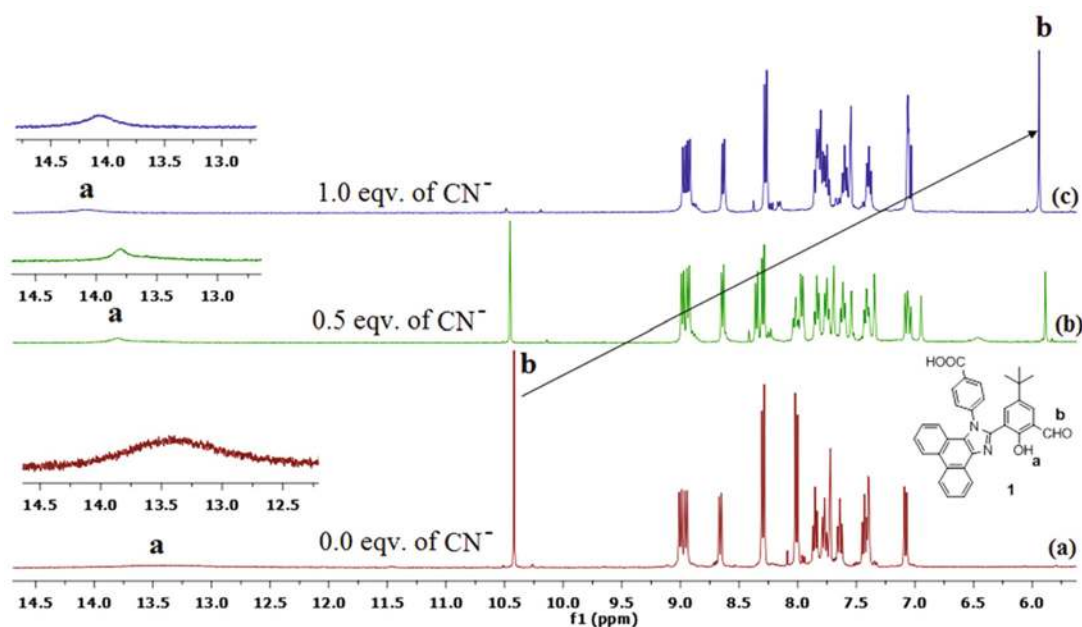
1454 | Photochem. Photobiol. Sci., 2018, **17**, 1450–1461

This journal is © The Royal Society of Chemistry and Owner Societies 2018

Fig. 7 Partial ^1H NMR spectra of compound **1** (3.07 × 10^{-2} M) in 0.3 mL of DMSO-d$_6$ in the presence of increasing concentration of CN$^-$. (a) 0.0 equiv. of CN$^-$, (b) 0.5 equiv. of CN$^-$, (c) 1.0 equiv. of CN$^-$.

with the oxygen (O$^-$) of cyanohydrin form. Formation of the cyanohydrin was further confirmed by LC mass spectrometry which gave m/z = 541.1953 corresponding to {**1-CN$^-$**} (Fig. S20 in ESI†).

Imidazole cyanohydrin {1-CN$^-$} compound for sensing Hg^{2+} ions

We investigated the reversible reaction of imidazole cyanohydrin {**1-CN$^-$**} with various biologically important metal ions such as Na$^+$, K$^+$, Mg^{2+}, Ca^{2+}, Mn^{2+}, Fe^{2+}, Co^{2+}, Ni^{2+}, Cu^{2+}, Zn^{2+} and Hg^{2+} (as perchlorate salts) in CH$_3$CN/H$_2$O (1:1, v/v) using absorption and fluorescence techniques. Notably, the weakly fluorescent solution of the **1-CN$^-$** adduct in CH$_3$CN/H$_2$O (1:1, v/v) turned strongly green fluorescent only in the presence of Hg^{2+} ions, whereas all other metal cations did not change the color of weak fluorescent light green in the solution. These changes further indicated a significant increase in the fluorescence intensity upon addition of Hg^{2+} ions to the **1-CN$^-$** derivative, and minimal changes in the presence of Cu^{2+} and Zn^{2+} (Fig. S24 in ESI†). This clearly showed that the **1-CN$^-$** derivative acts as a sensor for the detection of Hg^{2+}. Most likely this is a soft acid-soft base interaction. According to the HSAB theory,[21] CN$^-$ is a soft base and Hg^{2+} a soft acid and the interaction between soft acid and the soft base was stronger than other interactions (soft acid-hard base or *vice versa*).

We performed systematic titration studies of **1-CN$^-$** with addition of increasing equivalents of Hg^{2+} ions using absorption and emission techniques. The absorption spectral changes of **1-CN$^-$** with increasing amounts of Hg^{2+} ions in CH$_3$CN/H$_2$O (1:1 v/v) is shown in Fig. 8. The addition of increasing amounts of Hg^{2+} ions (0 to 4.0 equiv.) to a solution
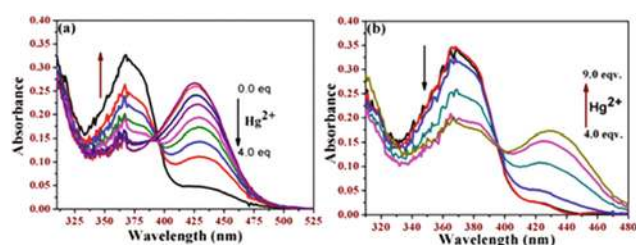

Fig. 8 Changes in absorption spectra of compound **1-CN$^-$** (10 μM) upon titration with Hg^{2+} (10 equiv.) in CH$_3$CN/H$_2$O (1:1). (a) Addition of 0 to 4.0 equiv., (b) 4.0 to 9.0 equiv. of Hg^{2+} ions.

of **1-CN$^-$** resulted in a decrease in the intensity of the absorption band at 425 nm and a simultaneous increase of the absorption bands at 370 nm with a clear isosbestic point at 392 nm, suggesting that **1-CN$^-$** and **1** were in equilibrium (Fig. 8a). Furthermore, the addition of larger amounts of Hg^{2+} ions (4.0 to 9.0 equiv.) to the solution resulted in an increase of the absorption band at 425 nm and a decrease of the absorption band at 370 nm (Fig. 8b). Next, we monitored the specific Hg^{2+} ion sensing phenomenon of **1-CN$^-$** by fluorescence titration studies. With the addition of increasing amounts of Hg^{2+} ions (0 to 4.0 equiv.) to **1-CN$^-$** the fluorescence emission band at 495 nm gradually increased and it reached the original fluorescence intensity of **1** as shown in Fig. 9a. Further increasing the amounts of Hg^{2+} ions (4.0 to 9.0 equiv.) resulted in a gradual decrease of the fluorescence emission and a bathochromic shift about 5 nm (Fig. 9b). This might be due to binding of Hg^{2+} to the imine nitrogen and oxygen atoms. To confirm this, we performed ^1H NMR titra-
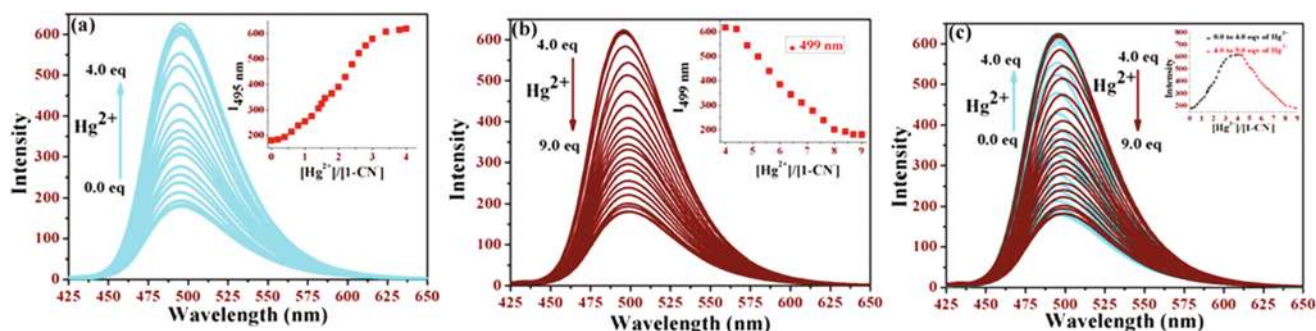
Fig. 9 Changes in emission spectra of compound **1-CN⁻** (10 μM) upon titration with Hg²⁺ (10 equiv.) in CH₃CN/H₂O (1 : 1) (λ_{ex} = 370 nm). (a) Addition of 0 to 4.0 equiv., (b) 4.0 to 9.0 equiv. of Hg²⁺ ions, and (c) overlay of both emission spectra. Insets show: plot of relative intensity maxima at 495 nm as a function of [Hg²⁺]/[**1-CN⁻**] molar ratio.

tion experiments of **1-CN⁻** with Hg²⁺ ions. Upon addition of 1.0 equiv. of Hg²⁺ ions, one observes signals characteristic for compound **1**, while the further addition of Hg²⁺ (2.0 equiv.) resulted in the disappearance of the signal for the hydroxy proton at 13.79 ppm (Fig. S25 in ESI†). This suggests that Hg²⁺ ions bind *via* the imine and oxygen units, which was further supported by ESI-MS studies (Fig. S26 in ESI†). Similar fluorescent titration changes were observed in the case of imidazole **2-CN⁻** (Fig. S27 in ESI†). Moreover, we tested imidazoles **1** and **2** with the addition of excess amounts of various other metal ions (Na⁺, K⁺, Mg²⁺, Ca²⁺, Mn²⁺, Fe²⁺, Co²⁺ and Ni²⁺). Neither induced any significant changes but minimal fluorescence changes were observed in the presence of Cu²⁺ and Zn²⁺.

Reversibility of the sensor

The reversibility and reusable response of imidazole **1** could be demonstrated during four cycles of titrations carried out with CN⁻ (weak fluorescence) followed by Hg²⁺ (strong fluorescence) in a sequence as shown in Fig. 10a. Furthermore, the CN⁻ induces a remarkable fluorescence change by showing

OFF behavior through cyanohydrin formation (**1-CN⁻**). Titration of cyanohydrin derivative with Hg²⁺ results in enhancing the fluorescence intensity and hence this acts as an ON switch. The repeated demonstration of OFF/ON behavior of the system by fluorescence as well as by the visual color change (inset Fig. 10) clearly suggests that imidazole **1** is reversible and a reusable sensor.

Conclusions

In conclusion, we prepared two novel substituted imidazoles **1** and **2** by standard reactions in high yields. The synthesized aldehyde imidazoles were treated with CN⁻ ions to form cyanohydrines, which quenched the fluorescence of the imidazole moiety (4-fold) and the singlet state lifetime decreased from 4.6 ns to 1.9 ns and 3.9 ns to 1.6 ns for compounds **1** and **2**, respectively. Additionally, ¹H NMR studies and Job's plot analyses revealed that CN⁻ binding involves the formation of a 1 : 1 cyanohydrin derivative between imidazole and CN⁻ ions which were further confirmed by LC-MS mass spectrometry. Therefore compounds **1** and **2** could serve as a highly sensitive and selective detector for CN⁻, with a detection limit of 0.8 μM and 1.2 μM in aqueous acetonitrile solution. The **1**-CN⁻ and **2**-CN⁻ derivatives were then used as fluorescence turn-on sensors to detect specifically Hg²⁺ ions over other cations, which can be a visually detected by a color change from yellow to colorless. The reversibility of imidazole **1** for sensing CN⁻ and Hg²⁺ ions has been demonstrated by repeated addition of these ions sequentially to complete four cycles in aqueous acetonitrile solution.

Experimental section

Chemicals

All the chemicals used for the synthesis were of reagent grade and solvents were dried by routine procedures immediately before use. Column chromatography was performed on silica gel Florisil (Merck, 200 mesh).
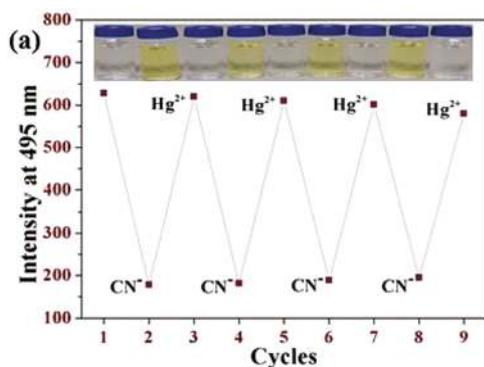
Fig. 10 Fluorescence experiment showing the reversibility and reusability of imidazole **1** for sensing CN⁻ and Hg²⁺ sequentially: (a) relative fluorescence intensity (λ_{max} at 495 nm) obtained during the titration of imidazole **1** with CN⁻ and Hg²⁺ in CH₃CN/H₂O (1 : 1). Above are the vials showing the visual color change at day light observed by naked eye.

1456 | *Photochem. Photobiol. Sci.*, 2018, **17**, 1450–1461

This journal is © The Royal Society of Chemistry and Owner Societies 2018

Instrumentation

All the NMR spectra were recorded using a Bruker AV 400 (400.23 MHz for ^{1}H NMR, 100.61 MHz for ^{13}C NMR) or Bruker AV 600 (600.13 MHz for ^{1}H NMR and 150.60 MHz for ^{13}C NMR) in CDCl$_3$ or DMSO-d$_6$. Absorption and steady-state fluorescence spectra were obtained with a Specord 250 spectrophotometer and Varian Cary-Eclipse instrument (λ_{ex} = 370 nm, and emission slit width = 2.5 nm), respectively. The fluorescence quantum yields were estimated from the emission and absorption spectra by a comparative method at an excitation wavelength of 370 nm using quinine bisulfate (φ = 0.55 in 1.0 N H$_2$SO$_4$)[22] as standard. The time-resolved fluorescence decay measurements were carried out at a magic angle using a picosecond diode laser-based time-correlated single photon counting (TCSPC) fluorescence spectrometer from IBH, UK. Infrared spectra were recorded on a Mattson Genesis II FTIR spectrophotometer equipped with a Gateway 2000 4DX2-66 workstation. HRMS spectra were measured with a MALDI-Q-TOF Premier Micromass and Micromass/WatersCorp. USA liquid chromatography time-of-flight spectrometer equipped with an electrospray ionization source (ESI). Melting points were acquired with a Stuart SMP-10 melting point apparatus and are uncorrected. For UV-Vis and fluorescence titration experiments, stock solutions of imidazole **1** and **2** (10 μM) was prepared by using spectroscopy grade CH$_3$CN–H$_2$O and (CH$_3$CH$_2$CH$_2$CH$_2$)$_4$N(CN) and Hg(ClO$_4$)$_2$ solutions (5 × 10^{-4} M) in CH$_3$CN–H$_2$O in 10 mL. The binding constant of the cyanohydrin derivatives formed in solution was estimated by using the standard Benesi–Hildebrand equation, *viz.*, $I_0/I = 1 + K[A]$; where I_0 is the intensity of the compound before addition of anion/cation, I is the intensity in the presence of anion/cation [A] and K is the association constant of the cyanohydrin derivative formed. For ^{1}H NMR titration experiments, the spectra were measured on a Bruker Advance 400 MHz spectrometer. A solution of **1** in DMSO-d$_6$ was prepared (3.02 × 10^{-2} M) and a 0.4 mL portion of this solution was transferred to a 5 mm NMR tube. Small aliquots of Bu$_4$NCN and Hg(ClO$_4$)$_2$ in DMSO-d$_6$ were added in an incremental fashion, and the corresponding spectra were recorded.

Syntheses

4-(2-(5-(*tert*-Butyl)-3-formyl-2-hydroxyphenyl)-1*H*-phenanthro[9,10-*d*]imidazol-1-yl)benzoic acid (1). The ester substituted imidazole **3** (0.500 g, 0.921 mmol) was dissolved in 20 mL of tetrahydrofuran/methanol (1 : 1 v/v) mixture, and KOH (0.206 g, 3.672 mmol) in 3 mL of H$_2$O was added to carry out the hydrolysis reaction under reflux for 6 h. After cooling to room temperature, the organic solvent was removed under reduced pressure, and the residue was diluted with 10 mL of distilled water. The resulting monopotassium salt of the corresponding imidazole carboxylic acid was collected by filtration. The monopotassium salt was acidified with concentrated HCl, followed by a thorough wash with hot water and a yellow powder of the imidazole carboxylic acid **1** was obtained in 92% yield (436 mg, 0.839 mmol). Mp: 308 °C; R_f = 0.48

(CH$_2$Cl$_2$/CH$_4$O, 1/1, v/v); ^{1}H NMR (400 MHz, dmso-d$_6$): δ = 13.45 (s, 1H, –OH), 10.41 (s, 1H, –CHO), 8.92 (dd, J = 8.9, 2.4 Hz, 2H, Ar), 8.61 (dd, J = 7.9, 1.1 Hz, 1H, Ar), 8.27 (dd, J = 8.2, 2.3 Hz, 2H, Ar), 7.95 (t, J = 10.6 Hz, 2H, Ar), 7.80 (dd, J = 11.1, 3.9 Hz, 1H, Ar), 7.76–7.65 (m, 2H, Ar), 7.59 (dd, J = 11.4, 4.2 Hz, 1H, Ar), 7.38 (t, J = 7.6 Hz, 1H, Ar), 7.30 (d, J = 7.2 Hz, 1H, Ar), 7.05 (d, J = 7.7 Hz, 1H, Ar), 0.98 ppm (s, 9H, –CH$_3$); ^{13}C NMR (101 MHz, dmso-d$_6$): δ = 191.31, 166.80, 159.27, 147.63, 142.23, 140.96, 134.77, 133.41, 132.14, 129.84, 129.29, 128.37, 127.56, 127.29, 126.83, 126.58, 126.34, 125.77, 125.15, 124.30, 123.22, 122.36, 120.81, 115.81, 34.08, 30.94 ppm; IR (ATR): ν_{max} (cm^{-1}) = 3223, 1682, 1596, 1474, 1445, 1377, 1263, 1220, 768, 693, 578; HRMS (ESI): *m/z* calcd for [C$_{33}$H$_{27}$N$_2$O$_4$] (M + H)$^+$ 515.1965; found 515.1976.

4-(2-(5-(*tert*-Butyl)-3-formyl-2-hydroxyphenyl)-4,5-diphenyl-1*H*-imidazol-1-yl)benzoic acid (2). The ester substituted imidazole **4** (0.500 g, 0.918 mmol) was dissolved in 20 mL of THF/methanol (1 : 1, v/v) mixture, and KOH (0.206 g, 3.672 mmol) in 3 mL of H$_2$O was added to carry out the hydrolysis reaction under reflux for 6 h. After cooling to room temperature, the organic solvent was removed under a reduced pressure, and the residue was diluted with 10 mL of distilled water. The resulting monopotassium salt of the corresponding imidazole carboxylic acid was collected by filtration. The monopotassium salt was acidified with concentrated HCl, followed by a thorough wash with hot water. Finally, a yellow powder of the imidazole carboxylic acid **2** was obtained in 90% yield (426 mg, 0.825 mmol). Mp: 265 °C; R_f = 0.48 (CH$_2$Cl$_2$/CH$_4$O, 1/1, v/v); ^{1}H NMR (400 MHz, dmso-d$_6$): δ = 13.36 (m, 1H, –OH), 10.45 (s, 1H, –CHO), 7.95 (t, J = 8.8 Hz, 2H, Ar), 7.63–7.58 (m, 3H, Ar), 7.45 (dd, J = 11.7, 4.5 Hz, 3H, Ar), 7.33–7.29 (m, 7H, Ar), 6.97 (d, J = 2.5 Hz, 1H, Ar), 0.88 ppm (s, 9H, –CH$_3$); ^{13}C NMR (101 MHz, dmso-d$_6$): δ = 190.33, 167.27, 159.25, 143.80, 131.72, 131.33, 130.91, 130.31, 129.43, 129.09, 129.02, 128.77, 128.63, 126.91, 126.67, 126.55, 124.89, 123.42, 115.97, 31.63, 30.93, 30.87 ppm; IR (ATR): ν_{max} (cm^{-1}) = 3218, 1682, 1657, 1599, 1477, 1381, 1263, 1216, 1169, 1008, 768, 697, 575; HRMS (ESI): *m/z* calcd for [C$_{33}$H$_{29}$N$_2$O$_4$] (M + H)$^+$ 517.2121; found 517.2127.

Ethyl 4-(2-(5-(*tert*-butyl)-3-formyl-2-hydroxyphenyl)-1*H*-phenanthro[9,10-*d*]imidazol-1-yl)benzoate (3). A solution of phenanthrene-9,10-dione (0.500 g, 2.4 mmol) and 5-*tert*-butyl-2-hydroxyisophthalaldehyde (0.495 g, 2.4 mmol) was added to acetic acid (30 mL). To this reaction mixture ethyl-4-aminobenzoate (0.397 g, 2.4 mmol) and ammonium acetate (0.555 g, 7.2 mmol) were added subsequently and refluxed for 12 h. The reaction mixture was cooled to room temperature and poured into water (80 mL) and extracted with ethyl acetate. The reaction mixture was concentrated to dryness under vacuum and the crude product was purified using silica gel column chromatography with hexane–ethyl acetate (5 : 95) and afforded pure ester substituted imidazole **3** as a yellow powder (0.949 g, 1.748 mmol, 73%). Mp: 295 °C; R_f = 0.70 (C$_6$H$_{14}$/C$_4$H$_8$O$_2$, 8/2, v/v); ^{1}H NMR (400 MHz, CDCl$_3$): δ = 13.89 (s, 1H, –OH), 10.54 (s, 1H, –CHO), 8.78 (d, J = 8.3 Hz, 1H, Ar–H), 8.72 (t, J = 8.0 Hz, 2H, Ar–H), 8.40 (d, J = 8.4 Hz, 2H, Ar–H), 7.76 (dd, J = 6.7, 2.2 Hz, 2H, Ar–H), 7.74–7.69 (m, 3H, Ar–H), 7.58–7.50 (m, 1H,

This journal is © The Royal Society of Chemistry and Owner Societies 2018

Photochem. Photobiol. Sci., 2018, **17**, 1450–1461 | **1457**

Ar–H), 7.31–7.27 (m, 1H, Ar–H), 7.21 (d, J = 6.9 Hz, 1H, Ar–H), 7.06 (d, J = 7.8 Hz, 1H, Ar–H), 4.51 (q, J = 7.1 Hz, 2H, –CH$_2$), 1.48 (t, J = 7.1 Hz, 3H, –CH$_3$), 1.02 ppm (s, 9H, –CH$_3$); ^{13}C NMR (101 MHz, CDCl$_3$): δ = 191.52, 165.25, 159.99, 147.42, 142.69, 140.94, 132.66, 132.04, 131.02, 129.67, 129.19, 128.54, 127.69, 127.07, 126.78, 126.40, 125.69, 124.38, 123.31, 122.70, 122.25, 120.76, 114.82, 61.87, 33.99, 30.90, 14.37 ppm; IR (ATR): ν_{max} (cm^{-1}) = 1678, 1596, 1470, 1420, 1277, 1263, 1169, 1108, 1001, 944, 772, 747, 718, 646, 607, 575; HRMS (MALDI): m/z calcd for [C$_{35}$H$_{31}$N$_2$O$_4$] (M + H)$^+$ 543.2284; found 543.2303.

Ethyl 4-(2-(5-(*tert*-butyl)-3-formyl-2-hydroxyphenyl)-4,5-diphenyl-1*H*-imidazol-1-yl)benzoate (4). A solution of benzil (0.500 g, 2.38 mmol) and 5-*tert*-butyl-2-hydroxyisophthalaldehyde (0.490 g, 2.38 mmol) was added to acetic acid (30 mL). To this reaction mixture ethyl-4-aminobenzoate (0.392 g, 2.38 mmol) and ammonium acetate (0.550 g, 7.14 mmol) were added subsequently and refluxed for 12 h. The reaction mixture was cooled to room temperature and poured into water (80 mL) and extracted with ethyl acetate. The reaction mixture was concentrated to dryness under vacuum and the crude product was purified using silica gel column chromatography with hexane–ethyl acetate (5 : 95) and afforded pure ester substituted imidazole **4** as pale-yellow powder (0.877 g, 1.610 mmol, 67%). Mp: 252 °C; R_f = 0.69 (C$_6$H$_{14}$/C$_4$H$_8$O$_2$, 8/2, v/v); ^{1}H NMR (400 MHz, CDCl$_3$): δ = 13.68 (s, 1H, –OH), 10.58 (s, 1H, –CHO), 8.09 (d, J = 8.4 Hz, 2H, Ar), 7.74 (d, J = 6.5 Hz, 1H, Ar), 7.56 (dd, J = 7.9, 1.3 Hz, 2H, Ar), 7.39–7.22 (m, 8H, Ar), 7.17 (dd, J = 7.9, 1.3 Hz, 2H, Ar), 7.02 (s, 1H, Ar), 4.41 (q, J = 7.1 Hz, 2H, –CH$_2$), 1.41 (t, J = 7.1 Hz, 3H, –CH$_3$), 0.97 ppm (s, 9H, –CH$_3$); ^{13}C NMR (101 MHz, CDCl$_3$): δ = 191.01, 165.18, 159.44, 143.99, 140.68, 131.17, 130.94, 130.41, 128.61, 127.34, 126.98, 123.40, 61.51, 33.82, 30.75, 14.21 ppm; IR (ATR): ν_{max} (cm^{-1}) = 1719, 1672, 1599, 1465, 1445, 1365, 1272, 1158, 1112, 1007, 944, 809, 770, 712, 692, 577; HRMS (ESI): m/z calcd for [C$_{35}$H$_{32}$N$_2$O$_4$] (M)$^+$ 545.2434; found 545.2427.

Crystal structure determinations

Single crystal X-ray diffraction data for all compounds were collected on a Bruker APEX 2 DUO CCD diffractometer by using graphite-monochromated MoK$_\alpha$ (λ = 0.71073 Å) radiation and Incoatec IµS CuK$_\alpha$ (λ = 1.54178 Å) radiation. Crystals were grown by dissolving the compounds in CH$_2$Cl$_2$ and layering with MeOH.[19] Crystals were mounted on a MiTeGen MicroMount and collected at 100(2) K by using an Oxford Cryosystems Cobra low-temperature device. All data were collected by using omega and phi scans and were corrected for Lorentz and polarization effects by using the APEX software suite.[23] Using Olex2, the structure was solved with the XT structure solution program, using the intrinsic phasing solution method and refined against |F^2| with XL using least squares minimisation.[24] Hydrogen atoms were generally placed in geometrically calculated positions and refined using a riding model. Details of data refinements can be found in Table S2 in ESI.† All images were prepared by using Olex2.

Crystal data for compound 2. C$_{35}$H$_{34}$N$_2$O$_5$S (M = 594.70 g mol^{-1}): monoclinic, space group $P2_1/c$ (no. 14), a = 9.5779(3) Å,

b = 29.6464(9) Å, c = 10.7257(3) Å, β = 92.205(2)°, V = 3043.31(16) Å^3, Z = 4, T = 100(2) K, μ(CuKα) = 1.315 mm^{-1}, D_{calc} = 1.298 g cm^{-3}, 38 472 reflections measured (5.962° ≤ 2θ ≤ 133.996°), 5433 unique (R_{int} = 0.0765, R_{sigma} = 0.0444) which were used in all calculations. The final R_1 was 0.0697 (I > 2σ(I)) and wR_2 was 0.1669 (all data). Donor H atoms were located and refined with restraints (DFIX).

Crystal data for compound 4. C$_{35}$H$_{32}$N$_2$O$_4$ (M = 544.62 g mol^{-1}): triclinic, space group $P\bar{1}$ (no. 2), a = 10.1174(6) Å, b = 10.6043(6) Å, c = 14.0472(8) Å, α = 83.9560(10)°, β = 72.1820(10)°, γ = 87.3180(10)°, V = 1426.66(14) Å^3, Z = 2, T = 100.0 K, μ(MoKα) = 0.083 mm^{-1}, D_{calc} = 1.268 g cm^{-3}, 69 783 reflections measured (3.06° ≤ 2θ ≤ 59.318°), 8057 unique (R_{int} = 0.0437, R_{sigma} = 0.0264) which were used in all calculations. The final R_1 was 0.0506 (I > 2σ(I)) and wR_2 was 0.1464 (all data). The *tert*-butyl group at C31 was modelled over two positions in an 83 : 14% occupancy using restraints (SIMU and SADI).

CCDC 1821473 (for **2**) and 1821472 (for **4**)† contain the supplementary crystallographic data for this paper.

Conflicts of interest

There are no conflicts to declare.

Acknowledgements

References

1 (*a*) P. D. Beer and P. A. Gale, Anion Recognition and Sensing: The State of the Art and Future Perspectives, *Angew. Chem., Int. Ed.*, 2001, **40**, 486–516; (*b*) C. Suksai and T. Tuntulani, Chromogenic anion sensors, *Chem. Soc. Rev.*, 2003, **32**, 192–202; (*c*) K. Choi and A. D. Hamilton, Macrocyclic anion receptors based on directed hydrogen bonding interactions, *Coord. Chem. Rev.*, 2003, **240**, 101–110; (*d*) F. P. Schmidtchen and M. Berger, Artificial Organic Host Molecules for Anions, *Chem. Rev.*, 1997, **97**, 1609–1646; (*e*) C. R. Bondy and S. J. Loeb, Amide based receptors for anions, *Coord. Chem. Rev.*, 2003, **240**, 77–99; (*f*) A. K. H. Hirsch, F. R. Fischer and F. Diederich, Phosphate Recognition in Structural Biology, *Angew. Chem., Int. Ed.*, 2007, **46**, 338–352; (*g*) S. W. Thomas III, G. D. Joly and T. M. Swager, Chemical sensors based on amplifying fluorescent conjugated polymers, *Chem. Rev.*, 2007, **107**, 1339–1386; (*h*) R. Martínez-Máñez and F. Sancenón, Fluorogenic and chromogenic chemosensors and reagents for anions, *Chem. Rev.*, 2003, **103**, 4419–4476; (*i*) Q. Zhao, F. Y. Li and C. H. Huang, Phosphorescent chemosensors based on heavy-metal complexes, *Chem. Soc. Rev.*, 2010, **39**, 3007–3030; (*j*) H. N. Kim, W. X. Ren, J. S. Kim and J. Yoon, Fluorescent and colorimetric sensors for detection of lead,

1458 | *Photochem. Photobiol. Sci.*, 2018, **17**, 1450–1461

This journal is © The Royal Society of Chemistry and Owner Societies 2018

cadmium, and mercury ions, *Chem. Soc. Rev.*, 2012, **41**, 3210–3244; (*k*) M. Kielmann, C. Prior and M. O. Senge, Porphyrins in troubled times: a spotlight on porphyrins and their metal complexes for explosives testing and CBRN defense, *New J. Chem.*, 2018, **42**, 7529–7550; (*l*) M. Kielmann and M. O. Senge, Molecular Engineering of Free Base Porphyrins as Ligands–The N-H···X Binding Motif in Tetrapyrroles, *Angew. Chem., Int. Ed.*, 2018, DOI: 10.1002/anie.201806281, in press.

2 (*a*) K. W. Kulig, *Cyanide Toxicity*, U. S. Department of Health and Human Services, Atlanta, GA, 1991; (*b*) M. A. Holland and L. M. Kozlowski, Clinical features and management of cyanide poisoning, *Clin. Pharm.*, 1986, **5**, 737–741.

3 World Health Organization, *Guidelines for Drinking-Water Quality*, World Health Organization, Geneva, 1996.

4 (*a*) F. Wang, L. Wang, X. Chen and J. Yoon, Recent progress in the development of fluorometric and colorimetric chemosensors for detection of cyanide ions, *Chem. Soc. Rev.*, 2014, **43**, 4312–4324; (*b*) P. A. Patnaik, *A Comprehensive Guide to the Hazardous properties of Chemical Substances*, van Nostrand Reinhold, New York, 1992, pp. 229–238; (*c*) J. J. Rosentreter, Y. G. Timofeyenko and M. Moreno, Safe routine cyanide detection methodology for aqueous solutions of varied pH, *Microchem. J.*, 2015, **119**, 17–21; (*d*) S. Bharadwaj and A. K. Singh, Visual & reversible sensing of cyanide in real samples by an effective ratiometric colorimetric probe & logic gate application, *J. Hazard. Mater.*, 2015, **296**, 54–60; (*e*) V. K. Gupta, A. K. Singh and N. Gupta, Colorimetric sensor for cyanide and acetate ion using novel biologically active hydrazones, *Sens. Actuators, B*, 2014, **204**, 125–135; (*f*) N. Yadav and A. K. Singh, Dual anion colorimetric and fluorometric sensing of arsenite and cyanide ions, *RSC Adv.*, 2016, **6**, 100136–100144.

5 (*a*) H. H. Harris, I. J. Pickering and G. N. George, The chemical form of mercury in fish, *Science*, 2003, **301**, 1203; (*b*) J. Gutknecht, Inorganic mercury (Hg^{2+}) transport through lipid bilayer membranes, *J. Membr. Biol.*, 1981, **61**, 61–66.

6 (*a*) M. Harada, Minamata disease: methylmercury poisoning in Japan caused by environmental pollution, *Crit. Rev. Toxicol.*, 1995, **25**, 1–24; (*b*) O. Brummer, J. J. La Clair and K. D. Janda, Practical screening of mercury contamination in fish tissue, *Bioorg. Med. Chem.*, 2001, **9**, 1067–1071; (*c*) G. Shanker, L. A. Mutkus, S. J. Walker and M. Schner, Methylmercury enhances arachidonic acid release and cytosolic phospholipase A2 expression in primary cultures of neonatal astrocytes, *Mol. Brain Res.*, 2002, **106**, 1–11; (*d*) E. K. Silbergeld, I. A. Silva and J. F. Nyland, Mercury and autoimmunity: implications for occupational and environmental health, *Toxicol. Appl. Pharmacol.*, 2005, **207**, 282–292; (*e*) A. Singh, T. Raj, T. Aree and N. Singh, Fluorescent Organic Nanoparticles of Biginelli-Based Molecules: Recognition of Hg^{2+} and Cl^- in an Aqueous Medium, *Inorg. Chem.*, 2013, **52**, 13830–13832; (*f*) P. Raj, A. Singh, A. Singh

and N. Singh, Syntheses and Photophysical Properties of Schiff Base Ni(ɪɪ) Complexes: Application for Sustainable Antibacterial Activity and Cytotoxicity, *ACS Sustainable Chem. Eng.*, 2017, **5**, 6070–6080; (*g*) M. Kaur, P. Raj, N. Singh, A. Kuwar and N. Kaur, Benzimidazole-Based Imine-Linked Copper Complexes in Food Safety: Selective Detection of Cyproheptadine and Thiabendazole, *ACS Sustainable Chem. Eng.*, 2018, **6**, 3723–3732.

7 Z. Xu, X. Chen, H.-N. Kim and J. Yoon, Sensors for the optical detection of cyanide ion, *Chem. Soc. Rev.*, 2010, **39**, 127–137.

8 (*a*) S. Saha, A. Ghosh, P. Mahato, S. Mishra, S. K. Mishra, E. Suresh, S. Das and A. Das, Specific Recognition and Sensing of CN^- in Sodium Cyanide Solution, *Org. Lett.*, 2010, **12**, 3406–3409; (*b*) H. Miyaji and J. L. Sessler, Off-the-Shelf Colorimetric Anion Sensors, *Angew. Chem., Int. Ed.*, 2001, **40**, 154–157; (*c*) P. Anzenbacher, D. S. Tyson, K. Jursikova and F. N. Castellano, Luminescence lifetime-based sensor for cyanide and related anions, *J. Am. Chem. Soc.*, 2002, **124**, 6232–6233.

9 (*a*) Y. Yang, Q. Zhao, W. Feng and F. Y. Li, Luminescent chemodosimeters for bioimaging, *Chem. Rev.*, 2013, **113**, 192–270; (*b*) R. Jackson, R. P. Oda, R. K. Bhandari, S. B. Mahon, M. Brenner, G. A. Rockwood and B. A. Logue, Development of a fluorescence-based sensor for rapid diagnosis of cyanide exposure, *Anal. Chem.*, 2014, **86**, 1845–1852; (*c*) K. P. Carter, A. M. Young and A. E. Palmer, Fluorescent sensors for measuring metal ions in living systems, *Chem. Rev.*, 2014, **114**, 4564–4601.

10 (*a*) Y. K. Yang and J. Tae, Acridinium salt based fluorescent and colorimetric chemosensor for the detection of cyanide in water, *Org. Lett.*, 2006, **8**, 5721–5723; (*b*) S. Park and H. J. Kim, Highly activated Michael acceptor by an intramolecular hydrogen bond as a fluorescence turn-on probe for cyanide, *Chem. Commun.*, 2010, **46**, 9197–9199; (*c*) Y. M. Dong, Y. Peng, M. Dong and Y. W. Wang, A selective, sensitive, and chromogenic chemodosimeter for cyanide based on the 1, 1′-binaphthyl scaffold, *J. Org. Chem.*, 2011, **76**, 6962–6966; (*d*) L. Yao, J. Zhou, J. Liu, W. Feng and F. Li, Iridium-Complex-Modified Upconversion Nanophosphors for Effective LRET Detection of Cyanide Anions in Pure Water, *Adv. Funct. Mater.*, 2012, **22**, 2667–2672; (*e*) K.-S. Lee, H.-J. Kim, G.-H. Kim, I. Shin and J.-I. Hong, Fluorescent chemodosimeter for selective detection of cyanide in water, *Org. Lett.*, 2008, **10**, 49–51.

11 (*a*) Y. K. Wu, X. J. Peng, J. L. Fan, S. Gao, M. Z. Tian, J. Z. Zhao and S. G. Sun, Fluorescence sensing of anions based on inhibition of excited-state intramolecular proton transfer, *J. Org. Chem.*, 2007, **72**, 62–70; (*b*) Y. Q. Xu and Y. Pang, Zinc binding-induced near-IR emission from excited-state intramolecular proton transfer of a bis (benzoxazole) derivative, *Chem. Commun.*, 2010, **46**, 4070–4072; (*c*) T. Kim, H. J. Kang, G. Han, S. J. Chung and Y. A. Kim, A highly selective fluorescent ESIPT probe for the dual specificity phosphatase MKP-6, *Chem. Commun.*, 2009, **45**, 5895–5897; (*d*) R. Hu, J. Feng, D. H. Hu, S. Q. Wang, S. Y. Li, Y. Li

This journal is © The Royal Society of Chemistry and Owner Societies 2018

Photochem. Photobiol. Sci., 2018, **17**, 1450–1461 | **1459**

and G. Q. Yang, A rapid aqueous fluoride ion sensor with dual output modes, *Angew. Chem., Int. Ed.*, 2010, **49**, 4915–4918; (*e*) Z. Xu, L. Xu, J. Zhou, Y. Xu, W. Zhu and X. Qian, A highly selective fluorescent probe for fast detection of hydrogen sulfide in aqueous solution and living cells, *Chem. Commun.*, 2012, **48**, 10871–10873; (*f*) D. P. Murale, H. Kim, W. S. Choi and D. G. Churchill, Highly selective excited state intramolecular proton transfer (ESIPT)-based superoxide probing, *Org. Lett.*, 2013, **15**, 3946–3949; (*g*) D. A. Yushchenko, J. A. Fauerbach, S. Thirunavukkuarasu, E. A. Jares-Erijman and T. M. Jovin, Fluorescent ratiometric MFC probe sensitive to early stages of α-synuclein aggregation, *J. Am. Chem. Soc.*, 2010, **132**, 7860–7861; (*h*) S. Goswami, A. Manna, S. Paul, A. K. Das, K. Aich and P. K. Nandi, Resonance-assisted hydrogen bonding induced nucleophilic addition to hamper ESIPT: ratiometric detection of cyanide in aqueous media, *Chem. Commun.*, 2013, **49**, 2912–2914; (*i*) A. C. Sedgwick, X. Sun, G. Kim, J. Yoon, S. D. Bull and T. D. James, Boronate based fluorescence (ESIPT) probe for peroxynitrite, *Chem. Commun.*, 2016, **52**, 12350–12352; (*j*) L. Chen, D. Wu, C. S. Lim, D. Kim, S.-J. Nam, W. Lee, G. Kim, H. M. Kim and J. Yoon, A two-photon fluorescent probe for specific detection of hydrogen sulfide based on a familiar ESIPT fluorophore bearing AIE characteristics, *Chem. Commun.*, 2017, **53**, 4791–4794; (*k*) L. Chen, D. Wu, J.-M. Kim and J. Yoon, An ESIPT-Based Fluorescence Probe for Colorimetric, Ratiometric, and Selective Detection of Phosgene in Solutions and the Gas Phase, *Anal. Chem.*, 2017, **89**, 12596–12601.

12 (*a*) S. J. Lim, J. Seo and S. Y. Park, Photochromic Switching of Excited-State Intramolecular Proton-Transfer (ESIPT) Fluorescence: A Unique Route to High-Contrast Memory Switching and Nondestructive Readout, *J. Am. Chem. Soc.*, 2006, **128**, 14542–14547; (*b*) J. Zhao, S. Ji, Y. Chen, H. Guo and P. Yang, Excited state intramolecular proton transfer (ESIPT): from principal photophysics to the development of new chromophores and applications in fluorescent molecular probes and luminescent materials, *Phys. Chem. Chem. Phys.*, 2012, **14**, 8803–8817.

13 (*a*) J. C. del Valle, R. M. Claramunt and J. Catalan, Fluorescence Spectroscopy and Amplified Spontaneous Emission (ASE) of Phenylimidazoles: Predicted Vibronic Coupling Along the Excited-State Intramolecular Proton Transfer in 2-(2′-Hydroxyphenyl)imidazoles, *J. Phys. Chem. A*, 2008, **112**, 5555–5565; (*b*) K. Y. Chen, C. C. Hsieh, Y. M. Cheng, C. H. Lai and P. T. Chou, Extensive spectral tuning of the proton transfer emission from 550 to 675 nm via a rational derivatization of 10-hydroxybenzo[h]quinoline, *Chem. Commun.*, 2006, 4395–4397; (*c*) K. I. Sakai, M. Ichikawa and Y. Taniguchi, Photoluminescent mechanism of a proton-transfer laser dye in highly doped polymer films, *Chem. Phys. Lett.*, 2006, **420**, 405–409.

14 J. E. Kwon, S. Park and S. Y. Park, Realizing molecular pixel system for full-color fluorescence reproduction: RGB-emit-ting molecular mixture free from energy transfer crosstalk, *J. Am. Chem. Soc.*, 2013, **135**, 11239–11246.

15 (*a*) S. Lochbrunner, K. Stock and E. Riedle, Direct observation of the nuclear motion during ultrafast intramolecular proton transfer, *J. Mol. Struct.*, 2004, **700**, 13–18; (*b*) S. Lochbrunner, A. J. Wurzer and E. Riedle, Ultrafast excited-state proton transfer and subsequent coherent skeletal motion of 2-(2′-hydroxyphenyl)benzothiazole, *J. Chem. Phys.*, 2000, **112**, 10699–10702; (*c*) S. Lochbrunner, A. J. Wurzer and E. Riedle, Microscopic Mechanism of Ultrafast Excited-State Intramolecular Proton Transfer: A 30 fs Study of 2-(2 '-Hydroxyphenyl) benzothiazole, *J. Phys. Chem. A*, 2003, **107**, 10580–10590.

16 (*a*) S. Kim, J. Seo, H. K. Jung, J. J. Kim and S. Y. Park, White Luminescence from Polymer Thin Films Containing Excited-State Intramolecular Proton-Transfer Dyes, *Adv. Mater.*, 2005, **17**, 2077–2082; (*b*) T. Mutai, H. Tomoda, T. Ohkawa, Y. Yabe and K. Araki, Switching of Polymorph-Dependent ESIPT Luminescence of an Imidazo [1, 2-a] pyridine Derivative, *Angew. Chem., Int. Ed.*, 2008, **47**, 9522–9524; (*c*) Y. Zhang, J.-H. Wang, W. Zheng, T. Chen, Q.-X. Tong and D. Li, An ESIPT fluorescent dye based on HBI with high quantum yield and large Stokes shift for selective detection of Cys, *J. Mater. Chem. B*, 2014, **2**, 4159–4166; (*d*) K. Dhanunjayarao, V. Mukundam and K. Venkatasubbaiah, A highly selective ratiometric detection of F⁻ based on excited-state intramolecular proton-transfer (imidazole) materials, *J. Mater. Chem. C*, 2014, **2**, 8599–8606; (*e*) K. Dhanunjayarao, V. Mukundam and K. Venkatasubbaiah, Ratiometric sensing of fluoride anion through selective cleavage of Si-O bond, *Sens. Actuators, B*, 2016, **232**, 175–180; (*f*) K. Dhanunjayarao, V. Mukundam and K. Venkatasubbaiah, Tetracoordinate Imidazole-Based Boron Complexes for the Selective Detection of Picric Acid, *Inorg. Chem.*, 2016, **55**, 11153–11159.

17 (*a*) K. Das, N. Sarkar, A. K. Ghosh, D. Majumdar, D. N. Nath and K. Bhattacharyya, Excited-state intramolecular proton transfer in 2-(2-hydroxyphenyl) benzimidazole and-benzoxazole: effect of rotamerism and hydrogen bonding, *J. Phys. Chem.*, 1994, **98**, 9126–9132; (*b*) P. Molina, A. Tarraga and F. Oton, Imidazole derivatives: A comprehensive survey of their recognition properties, *Org. Biomol. Chem.*, 2012, **10**, 1711–1724.

18 S. Park, O.-H. Kwon, S. Kim, S. Park, M.-G. Choi, M. Cha, S. Y. Park and D.-J. Jang, Imidazole-based excited-state intramolecular proton-transfer materials: synthesis and amplified spontaneous emission from a large single crystal, *J. Am. Chem. Soc.*, 2005, **127**, 10070–10074.

19 (*a*) H. Hope, X-Ray Crystallography: A Fast, First-Resort Analytical Tool, *Prog. Inorg. Chem.*, 1994, **41**, 1–10; (*b*) M. O. Senge, *Z.* A conformational study of 5, 10, 15, 20-tetraalkyl-22H⁺, 24H⁺-porphyrindiium salts (dication salts), *Z. Naturforsch.*, 2000, **55b**, 336–344.

20 L. Chen, S.-Y. Yin, M. Pan, K. Wu, H.-P. Wang, Y.-N. Fan and C.-Y. Su, A naked eye colorimetric sensor for alcohol

1460 | *Photochem. Photobiol. Sci.*, 2018, **17**, 1450–1461

This journal is © The Royal Society of Chemistry and Owner Societies 2018

vapor discrimination and amplified spontaneous emission (ASE) from a highly fluorescent excited-state intramolecular proton transfer (ESIPT) molecule, *J. Mater. Chem. C*, 2016, **4**, 6962–6966.

21 R. D. Hancock and A. E. Martell, Ligand design for selective complexation of metal ions in aqueous solution, *Chem. Rev.*, 1989, **89**, 1875–1914.

22 J. Olmsted, Calorimetric determinations of absolute fluorescence quantum yields, *J. Phys. Chem.*, 1979, **83**, 2581–2584.

23 (*a*) *SAINT, version 8.34a*, Bruker AXS, Inc., Madison, WI, 2013; (*b*) *SADABS, version 2014/5*, Bruker AXS, Inc., Madison, WI, 2014; (*c*) *APEX2, version 2014.11-0*, Bruker AXS, Inc., Madison, WI, 2014.

24 (*a*) O. V. Dolomanov, L. J. Bourhis, R. J. Gildea, J. A. K. Howard and H. Puschmann, OLEX2: a complete structure solution, refinement and analysis program, *J. Appl. Crystallogr.*, 2009, **42**, 339–341; (*b*) G. M. Sheldrick, Crystal structure refinement with SHELXL, *Acta Crystallogr., Sect. A: Found. Adv.*, 2015, **71**, 3–8.

This journal is © The Royal Society of Chemistry and Owner Societies 2018

Photochem. Photobiol. Sci., 2018, **17**, 1450–1461 | **1461**